THE ASTRONOMICAL JOURNAL, 121:2499–2514, 2001 May
© 2001. The American Astronomical Society. All rights reserved. Printed in U.S.A.

STRUCTURE AND KINEMATICS OF NGC 615 AND ITS NUCLEAR STAR FORMATION HISTORY[1]

O. K. SIL'CHENKO
Sternberg Astronomical Institute, Universitetskij Prospect 13, 119899 Moscow, and Instituto Isaac Newton, Moscow Branch, Russia; olga@sai.msu.su
V. V. VLASYUK
Special Astrophysical Observatory, Nizhnij Arkhyz, 357147 Karachai-Circessia, Russia; vvlas@sao.ru
AND
F. ALVARADO
Instituto Isaac Newton, Ministerio de Educación de Chile, Casilla 8–9, Correo 9, Santiago, Chile; falvarad@eso.org
Received 2000 May 5; accepted 2001 February 9

ABSTRACT

The results of a complex photometric and spectral investigation of the regular Sb galaxy NGC 615 are presented. The observations were made with the 6 m, 1 m, and 0.6 m telescopes of the Special Astrophysical Observatory RAS (Nizhnij Arkhyz, Russia) and the 1.5 m ESO telescope (La Silla, Chile). The analysis of the radial brightness profiles reveals the existence of at least two decoupled exponential components; the parameters of the outer component are typical for the global disks of Sb galaxies, and the inner component seen in the radius range 9″–30″ (1.0–3.5 kpc) is distinguished by compactness and high surface brightness. A combination of two-dimensional velocity fields for stars and ionized gas in the central part of the galaxy and of the long-slit velocity profiles along the major axis up to the optical border of NGC 615 provides some interesting findings. In the very center, $R < 3''$ (0.3 kpc), stars and gas rotate together, and the dynamical and photometric major axes are turned with respect to the global line of nodes; we conclude that an inclined circumnuclear disk is detected. In the bulge, $R = 3''$–$6''$ (0.35–0.75 kpc), the stellar velocity dispersion is more than 100 km s^{-1}, the stars rotate twice as slowly as the ionized gas, and a counterrotating gaseous component is observed. In the inner exponential component the stars rotate together with the ionized gas, and the stellar velocity dispersion drops to about 50 km s^{-1}. As the photometric major axis of this component is turned with respect to the line of nodes, we call it "an oval inner disk." The mean age of the stellar populations in the nucleus and in the inner disk beyond its H II regions is 5 Gyr, while the bulge is much older. Both the chemically decoupled nucleus of NGC 615 and the inner disk probably formed the bulk of their more luminous stars in a secondary burst of star formation, perhaps provoked by the close passage of another galaxy some gigayears ago.

Key words: galaxies: nuclei — galaxies: individual (NGC 615) — galaxies: evolution — galaxies: structure — galaxies: kinematics and dynamics

1. INTRODUCTION

Despite the rapid development of observational techniques and extensive photometric surveys of spiral galaxies undertaken with CCDs (among the most recent examples, see de Jong 1996; Moriondo, Giovanardi, & Hunt 1998; Courteau 1996), the simplified view of the structure of spiral galaxies is still common. One continues to consider a spiral galaxy (at least of the SA type) as consisting of two main components, namely, a bulge and a disk, following the early suggestion of Hubble (1926). Meanwhile, during the epoch of intensive surface photometry, there was always evidence of a more complex structure in normal disk galaxies. For example, many galaxies are known to have so-called lenses between their bulges and disks. Sometimes a lens is certainly something disklike and contains spirals, as in NGC 6654 (Kormendy 1977); sometimes a lens is dynamically hot, even hotter than the bulge, as in NGC 1553 (Kormendy 1984). Up to now, there have been no definitive conclusions about the nature of lenses apart from the hypothesis of Kormendy (1979), that they may be a product of bar decays. Also known are several other clear cases in which the brightness profile of a global galactic disk consists of two exponential segments with different scale lengths: NGC 3642 (Boroson 1981), NGC 5533 (Sil'chenko, Burenkov, & Vlasyuk 1997), and NGC 157 (Ryder et al. 1998). Recently, we undertook a detailed study of an isolated unbarred Sab galaxy, NGC 7217 (Sil'chenko & Afanasiev 2000). We divided the surface brightness profile of this galaxy into three exponential segments with different scale lengths: two disks, recognized by the low stellar velocity dispersion, and an exponential bulge. Once again, the intermediate, probably oval, disk may be a product of bar decay, because this face-on unbarred galaxy shows three stellar rings, which one usually relates to resonance locations of a bar (Buta et al. 1995). Now we report a study of another spiral galaxy, NGC 615, which resembles NGC 7217 in many respects as will be shown below.

NGC 615 is a regular early-type spiral galaxy: it is characterized as SA(rs)b in the NASA/IPAC Extragalactic Database (NED). The galaxy's main characteristics are given in Table 1. De Vaucouleurs & de Vaucouleurs (1964) noted a bright ring in NGC 615 with a size of 0.′7 × 0.′2, which is a strange finding, since rings are usually observed in barred galaxies and are thought to be located on bar resonances (Buta 1993; Buta & Crocker 1993). Many years ago we began a study of gas kinematics in NGC 615, considering this galaxy as a prototype of unbarred Sb's. Our first major-axis profile for this galaxy (Afanasiev et al. 1988), though not of a very high quality, nevertheless revealed a

[1] Based on observations collected with the 6 m, 1 m, and 0.6 m telescopes of the Special Astrophysical Observatory (SAO) of the Russian Academy of Sciences (RAS) and with the 1.52 m ESO telescope at La Silla.

TABLE 1

GLOBAL PARAMETERS OF NGC 615

Parameter	Value
Type (NED)	SA(rs)b
R_{25}, kpc (LEDA)	11.1
B_T^0 (LEDA)	11.77
M_B (LEDA)	−20.15
$B-V$ (RC3)	0.86
$U-B$ (RC3)	0.28
V_{sys}(radio) (LEDA), km s^{-1}	1846 ± 4
Distance, Mpc (LEDA, $H_0 = 75$ km s^{-1} Mpc^{-1})	24
	so 1″ = 0.116 kpc
Inclination (LEDA)	71°
P.A.$_{phot}$ (NED)	155°
v_{rot} (km s^{-1}) (LEDA)	193

steep central velocity gradient within an unresolved core radius that allowed us to include NGC 615 in our list of spiral galaxies with kinematically decoupled nuclei (Afanasiev, Sil'chenko, & Zasov 1989). The galaxy was never classified as barred; despite this fact, we have undertaken an additional test of the circular character of the gas rotation in its center. A two-dimensional velocity field of the ionized gas was obtained by measuring the emission line [N II] λ6583 within $R \approx 4''$ with an early variant of the multipupil spectrograph of the 6 m telescope equipped with a photon-counting system; the direction of the maximum line-of-sight velocity gradient was found to be P.A. ≈ 160° (Sil'chenko 1994). Since the orientation of the inner isophotes obtained with the spatial resolution of 2.″5 is P.A.$_{in} = 156° \pm 2°$ (Sil'chenko & Vlasyuk 1992) and does not differ from the outer line-of-nodes P.A.$_0 = 155°$ (NED), we concluded that the circumnuclear ionized gas in NGC 615 exhibits circular rotation in the main galactic plane, and its steep central velocity gradient is probably caused by a strong mass concentration in the unresolved core. The dynamical distinctness of the nucleus of NGC 615 stimulated our interest in the stellar population properties in the nucleus and its outskirts. We observed the galaxy in the Mg *b* spectral range during our first observational run with the multipupil spectrograph of the 6 m telescope and immediately found a magnesium-line equivalent-width drop between the nucleus and the bulge (Sil'chenko, Afanasiev, & Vlasyuk 1992). Obviously, the nucleus of NGC 615 is decoupled both dynamically and chemically and must have a proper evolution. We decided to continue a study of the structure and kinematics of this galaxy to reveal its (unusual?) features, which may be consequences of minor merger events or, on the contrary, may be intrinsic stimulators of the decoupled nucleus formation (e.g., evidencing some triaxiality). In this work, we present results of the complex photometric and spectral investigation of this interesting, though in many respects quite regular, spiral galaxy. We report our observations and their reduction details in § 2. The photometric structure of NGC 615 is studied in § 3, and the kinematic analysis is presented in § 4. The radial variations of the stellar population properties are analyzed in § 5. Section 6 gives some concluding remarks.

2. OBSERVATIONS AND DATA REDUCTION

Since 1994, when the multipupil field (MPFS) spectrograph of the 6 m telescope (Afanasiev et al. 1990, 1996) was equipped with a 520 × 580 CCD detector, the accuracy of measurements has been substantially improved, so we reobserved NGC 615 with the MPFS in 1998 to obtain stellar and gaseous kinematics and stellar population characteristics for the central region. To extend our analysis beyond the central region, we have also obtained long-slit profiles along the major axis and broadband *BVRI* images.

The detailed parameters of the MPFS observations are given in Table 2. The MPFS allows us to obtain a set of about 100 spectra from a rectangular area of an extended astronomical object (e.g., of a galaxy). We have obtained two such sets for the central region of NGC 615. One is obtained in the green spectral range, 4800–5400 Å, which we have used to derive a two-dimensional velocity field of stars by cross-correlating individual spectra with spectra of bright K giant stars and to calculate absorption-line indices in the Lick system (it includes several strong absorption lines, Hβ, Mg I *b*, Fe I λ5270, and Fe I λ5335, which can be used for diagnostics of the stellar population properties). Another is obtained in the red, 6200–6900 Å—it contains emission lines, in this particular case [N II] λ6583, which is used to calculate a two-dimensional velocity field of the ionized gas. These observations have been performed with a reciprocal dispersion of 1.6 Å pixel^{-1} (the spectral resolution of 4–6 Å slightly varying over the frame). To calibrate the wavelength scale, we exposed separately a spectrum of the hollow-cathode lamp filled with helium, neon, and argon, and the accuracy of the calibration was also checked by measuring positions of night-sky emission lines. In the red, the velocities were corrected for the systematic velocity shift of 45 km s^{-1} derived from the measurements of sky emission line [O I] λ6300. The mean random error of an individual measurement of a weak emission line is 19 km s^{-1}. The elementary stellar velocities are also measured with the accuracy of some 20 km s^{-1}. To account accurately for the night-sky background in the green spectral range for equivalent width calculations, we have separately exposed the blank-sky region at 2′ from the galaxy with an exposure time of one-half that for the galaxy; the sky was then (after spectrum extraction and linearization) smoothed and subtracted. The absorption-line indices Hβ, Mg *b*, Fe5270, and Fe5335 have been calculated in the standard Lick system (Worthey et al. 1994). We have checked our consistency with the Lick measurements by observing nine stars from the list of Worthey et al. (1994) and by calculating the absorption-line indices for the stars in the same manner as for the galaxies. The indices calculated for the stars are coincident with the data tabulated in

TABLE 2

TWO-DIMENSIONAL SPECTRAL OBSERVATIONS OF NGC 615

Date	Exposure (minutes)	Field (arcsec)	Scale	Spectral Range (Å)	P.A.(top) (deg)	Seeing (arcsec)
1998 Jan 20.....	90	10.4 × 15.6	1.″3/lens	6200–6900	63	2.4
1998 Jan 21.....	60	10.4 × 15.6	1.″3/lens	4700–5450	63	2.4

TABLE 3

PHOTOMETRIC CCD OBSERVATIONS OF NGC 615

Date	Telescope	Filter	Exposure (s)	Seeing (arcsec)	Scale (arcsec)
1998 Jan 3.....	SAO 1 m	*B*	1800	3.0	0.28 × 0.37
		V	600	3.0	0.28 × 0.37
		R	600	3.0	0.28 × 0.37
		I	600	2.8	0.28 × 0.37
2000 Oct 3.....	SAO 0.6 m	*V*	500	2.6	0.45 × 0.45
		R	300	1.9	0.45 × 0.45
2000 Oct 6.....	SAO 0.6 m	*B*	570	2.0	0.45 × 0.45
		V	540	1.8	0.45 × 0.45
		R	60	2.1	0.45 × 0.45
		I	450	2.0	0.45 × 0.45

Worthey et al. (1994) in average within 0.05 Å. The exposure time for the galaxy has been taken long enough to provide a signal-to-noise ratios of ~ 60 Å^{-1} in the nucleus and ~ 30 Å^{-1} near the edges of the frames; the corresponding random error estimations made in the manner of Cardiel et al. (1998) range from 0.15 Å in the center to 0.6 Å for the individual spatial elements in the outer part. To keep a constant level of accuracy along the radius, we summed the elementary spectra in concentric rings centered onto the nucleus and studied the radial dependencies of the absorption-line indices by comparing them to synthetic models of old stellar populations of Worthey (1994) and Tantalo, Chiosi, & Bressan (1998). We estimate the mean accuracy of our azimuthally averaged indices as 0.1 Å.

To refine mainly a kinematic analysis, we have also obtained long-slit spectra of NGC 615 with the Boller & Chivens spectrograph of the 1.5 m ESO telescope in La Silla. The galaxy was exposed for 3 hr on 1998 August 12/13 and for 4 hr on 1998 August 13 and 14. The slit has been aligned with the major axis of the galaxy, at P.A. = 154°. The 2048 × 2048 Loral CCD was used as a detector: the scale along the slit was 0.″82 pixel^{-1}, the slit width during the galaxy exposure was 1.″5 matched to the seeing quality, also of 1.″5. The spectral range is 4730–6780 Å with the reciprocal dispersion of 1 Å pixel^{-1}, so it includes the main absorption lines under consideration, as well as the emission lines Hα and [N II] λ6583. As a template for cross-correlation and as a standard of Lick indices, we also observed a K0 giant star, HD 172401. Since the spectral resolution of our long-slit observations, ~ 2.5 Å, differs strongly from the standard Lick system resolution, ~ 8 Å, we have investigated the stellar velocity dispersion influence on the Lick index measurements by broadening the HD 172401 spectrum with Gaussians of different σ. When calculating the Lick indices for NGC 615, we applied the correction for the stellar velocity dispersion and the correction for the spectral resolution, which has appeared to be -0.4 Å for Mg *b*, Fe5270, and Fe5335, and zero for Hβ as determined by differences of our measurements for HD 172401 and the tabular values from Worthey et al. (1994). The latter corrections have been also checked by comparing the Lick indices calculated for the twilight sky from the long-slit data

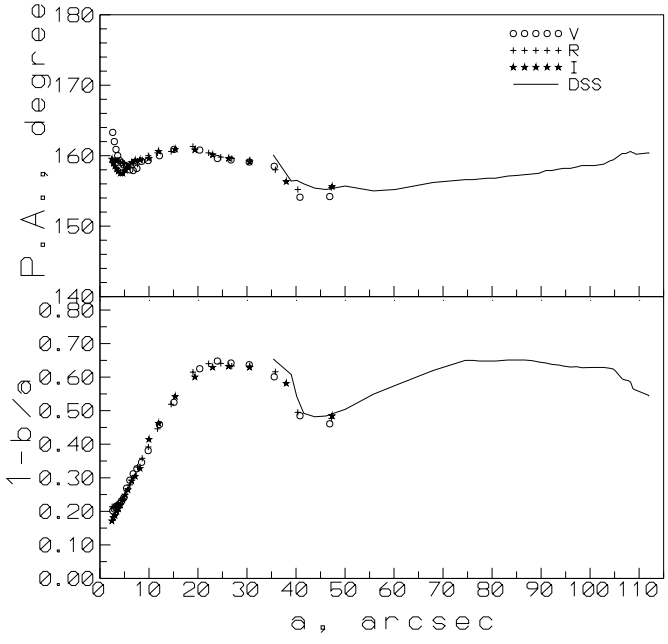


FIG. 1*a*

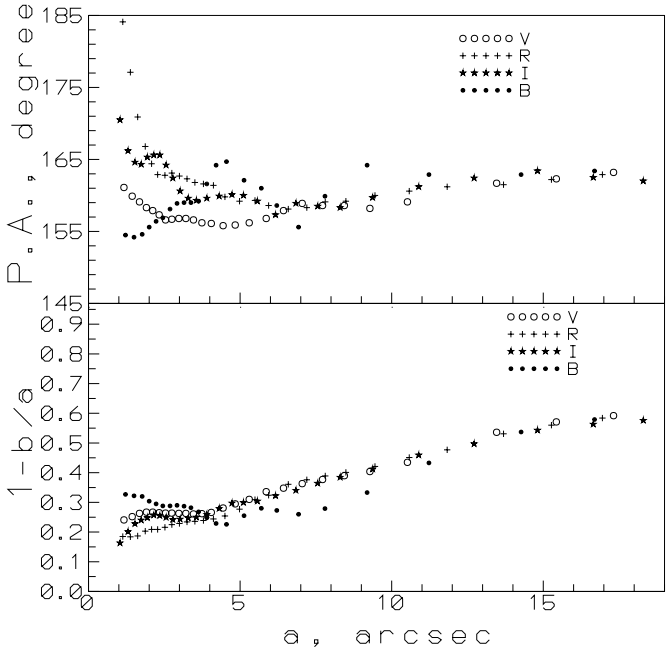


FIG. 1*b*

FIG. 1.—Radial variations of the isophote morphological characteristics in NGC 615 (*a*) in the full radius range, according to our *VRI* data of 1998 and as obtained from the DSS image in the outer part, and (*b*) in the central part of the galaxy, according to our *BVRI* data of 2000 October 6.

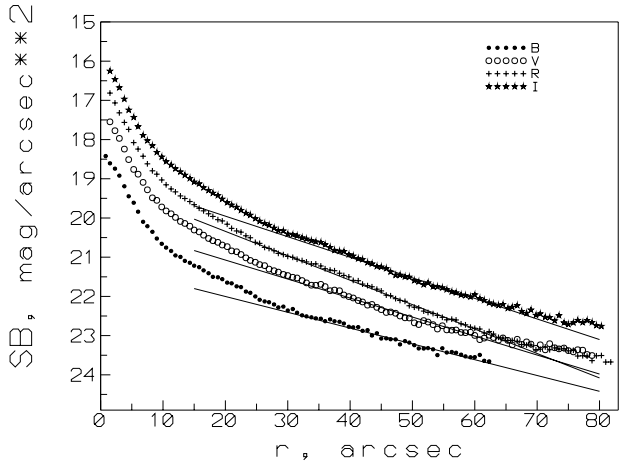


FIG. 2.—Azimuthally averaged brightness profiles in the *BVRI* passbands according to our data of 1998; the invalidity of the exponential fit to the outermost parts of the profiles at $R < 30''$–$35''$ illustrates the multicomponent structure of NGC 615.

and from our MPFS observations. The wavelength calibration of the long-slit spectra was made with the accuracy better than 0.1 Å, and our measurements of the sky emission line [O I] λ6300 have confirmed that the velocities from the emission lines are measured with rms errors smaller than 10 km s^{-1}. However, a systematic shift of 30 km s^{-1} was observed in the first night of our long-slit observations.

The photometric observations of NGC 615 were performed with the 1 m and 0.6 m telescopes of the Special Astrophysical Observatory. The 520 × 580 CCD detector with 18 × 24 μm pixels at the 1 m telescope and the 1040 × 1160 CCD with the square 16 μm pixels at the 0.6 m telescope were used. The observations were made through *BVRI* filters and on photometric nights. To obtain the photometric standards, we exposed a field from Landolt (1992), PG 0231. The detailed parameters of our photometric observations are given in the Table 3.

The galaxy and the standard field have been observed at different zenith distances. So, after calibrating the images into the standard Johnson-Cousins photometric system by using the standard field exposures, we have checked our calibration with the multiaperture photometric data taken from HYPERCAT. They include the *BV* photoelectric estimates from Longo & de Vaucouleurs (1983), Véron-Cetty (1984) and an *I*-band profile recalculated into a homogeneous set of apertures from Mathewson & Ford (1996). The *BV* calibrations appeared to be consistent according to both approaches, and the *I* calibration by PG 0231 for the data of 1998 showed a zero-point shift of 0.18 mag with respect to that basing on the Mathewson & Ford (1996) data. We do not know the cause of this shift, but the calibration of the data from 0.6 m telescope confirms that the calibration of Mathewson & Ford (1996) is correct. So we have preferred to use the calibration from the multiaperture photometry of NGC 615 as more safe for the *I* band only.

Finally, for the illustrative purposes we use also data obtained for the NGC 615 through the narrow filter centered onto the redshifted Hα at the scanning Fabry-Pérot interferometer of the 6 m telescope during the observations in the frame of the program on spiral galaxy kinematics (Principal Investigator Professor A. M. Fridman). The galaxy was observed on 1998 August 29, during 72 minutes, with the 235th-order etalon; the filter's FWHM was 10.2 Å, the spatial bin was 0.″68 per CCD pixel, and the seeing quality was 1.″5.

All the data, both spectroscopic and photometric, have been reduced using software developed in the Special Astrophysical Observatory (Vlasyuk 1993).

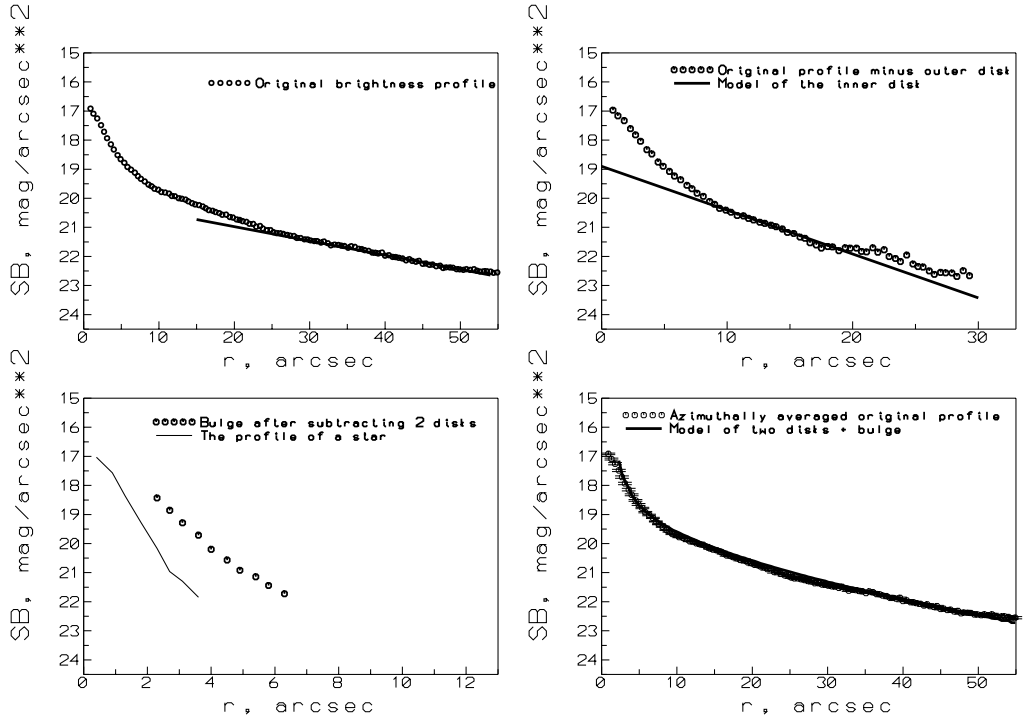


FIG. 3.—Step-by-step decomposition of the azimuthally averaged brightness profile shown by the example of the *V* profile obtained on 2000 October 6. The seeing was 1.″8. The profile of a neighboring star is given as a solid line on the bottom left plot.

3. PHOTOMETRIC STRUCTURE OF NGC 615

As we have already mentioned (see Table 1), the galaxy is classified by a type of SA(rs)b; so, being unbarred it would have to demonstrate a simple two-component structure, and being an early-type spiral it would have to possess a noticeable de Vaucouleurs' bulge. With our photometric data we are able to check whether it is so.

Figure 1 presents radial variations of the isophote characteristics obtained by fitting the isophotes in various passbands by ellipses. Our own observations allow us to trace the isophote parameters up to $R \approx 50''$; to extend the analysis up to the optical border of the galaxy we have used the Digitized Sky Survey (DSS) data. One can see that the position angle of the isophote major axis varies quite weakly and is confined to the range of 155°–160° over the whole radius range. This constancy confirms a claimed axisymmetry of NGC 615. However, an accuracy of our position angle determinations is better than 1° (which can be seen from the excellent agreement of the measurements in different passbands), and variations of P.A. from 160° at $R \approx 20''$ to 155° at $R \approx 60''$ and again to 160° at $R \geq 100''$, must be considered as significant. A curious behavior is found for the isophote ellipticity. In the very center (Fig. 1*b*), it demonstrates a plateau at $R = 2''$–$4''$ instead of going to zero as appropriate for spheric bulges. Farther from the center its behavior is also nonmonotonic: twice, at $R \approx 20''$ and at $R \geq 70''$, it reaches 0.6—a value suitable for a thin disk inclined by some 70° (LEDA: $i = 71°$; Bottinelli et al. 1984: $i = 66°$), but in the transition zone, at $R \approx 40''$–$50''$, it is only 0.48, implying an inclination less than 60°. What is the true inclination and orientation of the galactic plane? If $i = 70°$ and P.A. = 160°, what do we see at $R = 40''$–$50''$? The global structure of NGC 615 promised to be interesting.

The surface brightness radial profile of NGC 615 was already measured in the *I* passband by Mathewson & Ford (1996) as part of a sample of more than 2400 galaxies; no particular analysis was attached. The visual inspection of their Figure 1 allows us to conclude that the photometric profile of NGC 615 is rather complex and cannot be fitted by a simple two-component model. One can note at least two points where the profile slope changes abruptly, so there are at least three distinct components of the galactic structure. The brightness profiles obtained by us in four photometric passbands (Fig. 2) show at least two exponential segments with different slopes: in the radius ranges of 10″–30″ and 40″–70″. As our isophotal analyses has shown

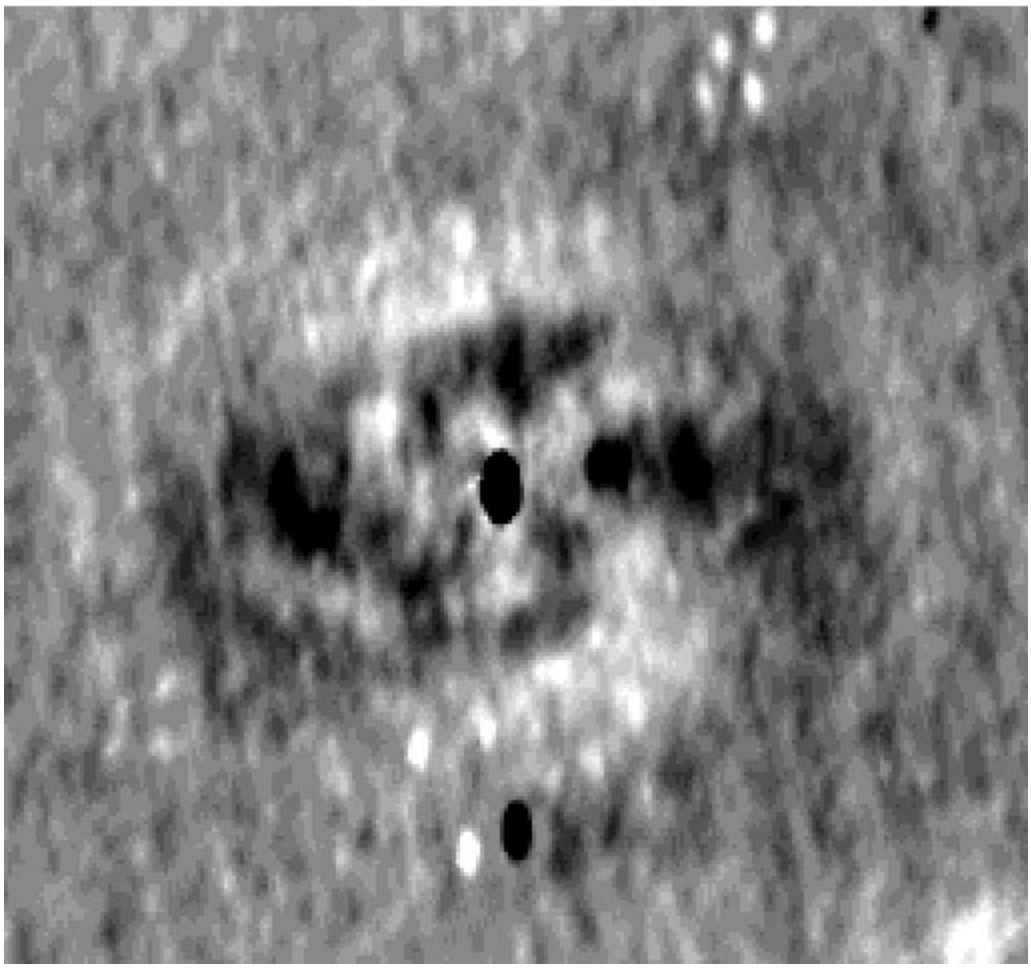


FIG. 4*a*

FIG. 4.—Residual brightness maps of the central part 100″ × 100″ of NGC 615 deprojected onto the galactic plane; from the original images were subtracted the model exponential outer disk and smooth elliptical isophote models for the inner disk and the bulge. The line of nodes has been turned to the horizontal direction, and then the image was scaled in the vertical direction to match the inclination of ~ 60°. The red star image on the bottom of *I* map gives an impression about PSF. (*a*) *I*-band data, (*b*) *V*-band data, (*c*) *B*-band data, all from 2000 October 6.

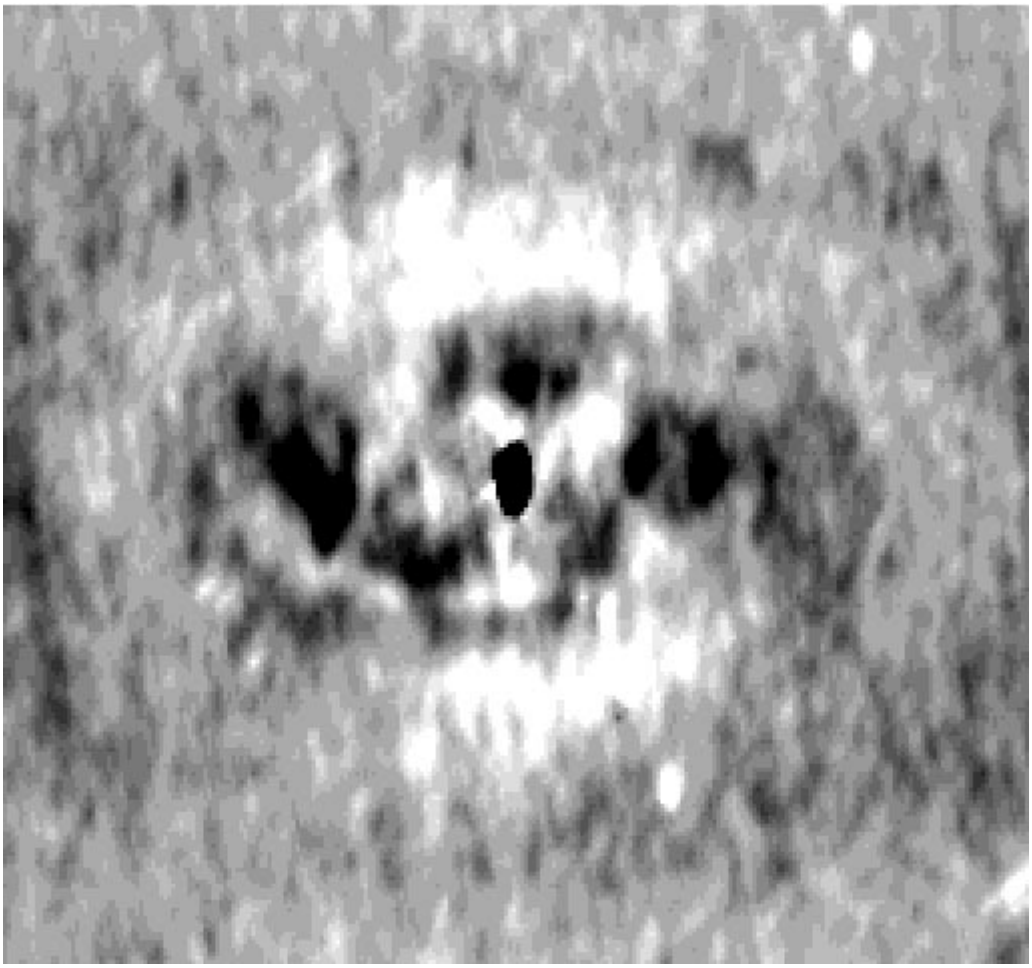


FIG. 4*b*

(Fig. 1*a*), the orientation of the major axis changes abruptly between these components. We have already known galaxies with two exponential disks differing by their scale lengths and central brightnesses: in NGC 5533 (Sil'chenko et al. 1997), the innermost of two disks that have been traced up to $R \approx 13$ kpc demonstrates quite normal characteristics, whereas the more outer disk is very extended and belongs to a class of low surface brightness galactic disks. In the case of NGC 615, the situation looks substantially different: three photometric components are all seen within $R \approx 11$ kpc. We begin fitting the brightness profiles with their outer parts, subsequently subtracting the two-dimensional model images from the images of the galaxy. An example of this step-by-step fitting made for the *V*-band data of 2000 October 6 is presented in Figure 3, and the results of the brightness profile fitting in all four filters are given in Table 4. For every structural component, a separate isophote analysis was performed to determine a position angle and ellipticity for ellipse averaging of the brightness profiles. If the ellipticity varied along the radius

TABLE 4

PARAMETERS OF THE BRIGHTNESS PROFILE FITTING

Component	Radius Range of Fitting (arcsec)	P.A.$_0$ (deg)	b/a	μ_0 (mag arcsec^{-2})	r_0 (arcsec)	r_0 (kpc)
B band:						
Outer disk.....	40–60	158	0.52	21.2	27.0	3.1
Inner disk	7–19	163	0.57	19.7	7.9	0.9
V band:						
Outer disk.....	40–60	158	0.52	20.1	22.6	2.6
Inner disk	9–24	163	0.52	18.8	7.2	0.8
R band:						
Outer disk.....	40–66	158	0.52	19.1	17.5	2.0
Inner disk	9–20	163	0.50	18.2	6.9	0.8
I band:						
Outer disk.....	40–65	158	0.52	18.9	20.7	2.4
Inner disk	10–28	165	0.44	17.8	8.2	0.95

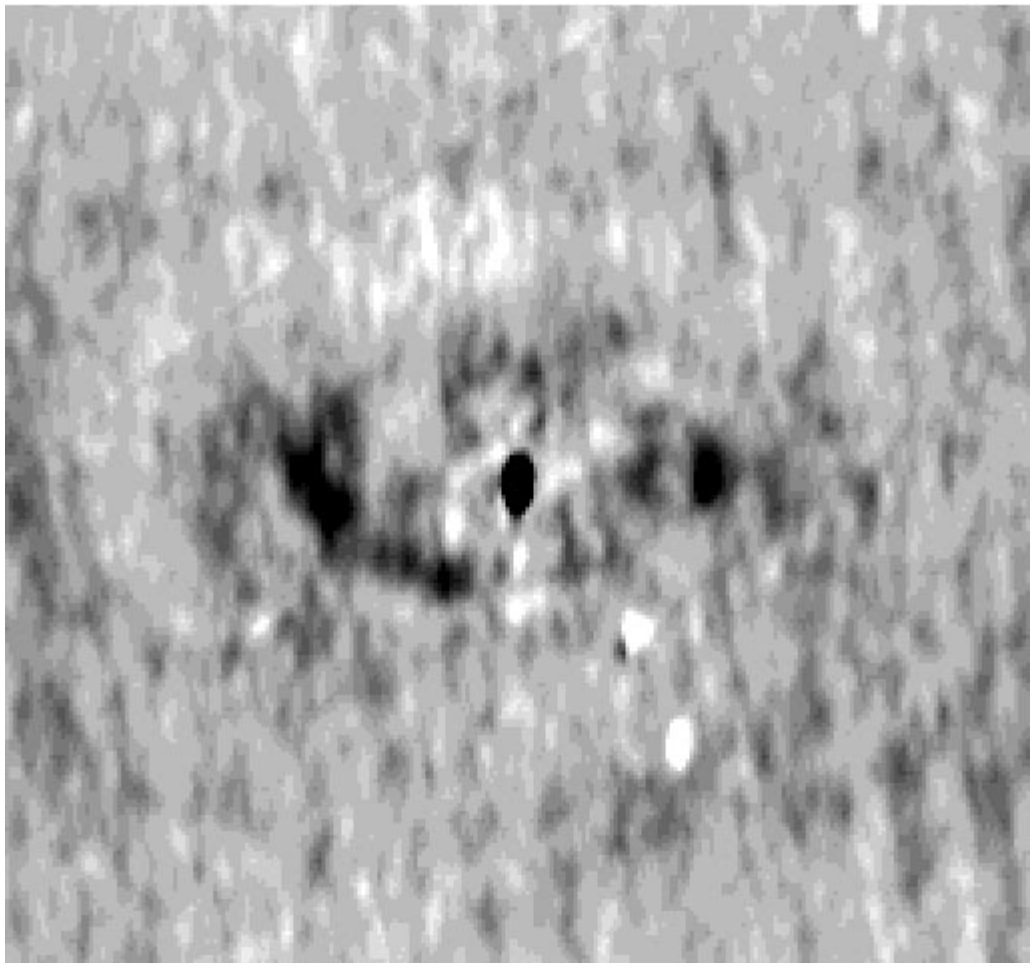


FIG. 4*c*

within one structural component, we took the minimum value to avoid confusion by intrinsically elliptical rings. For the parameters of the outer component we prefer to use the observations of 1998 as more deep; for the inner component we give a higher weight to the data of 2000 October 6, as obtained under the best seeing. However, the analysis of data from all three nights has shown their consistency as concerning the parameters of the exponential components.

The outer disk of NGC 615 appears to be quite normal for a Sb galaxy with its scale length 2–3 kpc and the central surface brightness, $\mu_0 = 21.2 \pm 0.2$ B mag arcsec^{-2}, only slightly brighter than the standard Freeman (1970) value, 21.65. The residual image, after subtracting the outer disk, demonstrates a pair of low-contrast outer spirals or, more likely, a ring, more prominent in the red passbands, I and R. The inner exponential component, fitted to the residual image in the radius range of 9″–25″ after subtracting the first disk and masking the bright spots on the major axis, has a somewhat different orientation of the line of nodes—P.A. = 163° instead the mean outer P.A. = 158°—it is very bright and compact, with the exponential scale length of 7″–8″ (0.9–1.0 kpc). When this component has been also subtracted, the remaining innermost part of the residual profile does not contradict an interpretation of a quasi-spheric de Vaucouleurs bulge, though with the extreme compactness ($r_e \approx 0\farcs6$, or less than 100 pc); the exact determination of the bulge's structural parameters is difficult with our spatial resolution. A comparison of the observed V brightness profile with the three-component model (two exponentials plus de Vaucouleurs bulge; Fig. 3, *bottom right*) shows a perfect agreement from the nucleus up to $R \approx 70''$ (8 kpc); the same is true for all the passbands. So we conclude that an existence of two exponential stellar components with different scale lengths in NGC 615 is rather evident. To reveal the nature of the inner component, one must appeal to dynamical arguments. The measurements of the stellar velocity dispersion are reported in the next section, but now we can conclude something from the morphology of the residual brightness distribution. The residual images, obtained by subtracting the outer model disk and smooth elliptical isophotes fitting the inner components and deprojected onto the galactic plane, are shown in Figure 4. A set of bright spots near the center demonstrates a ringlike distribution with a radius of approximately 10″–13″. One can also see a prominent two-armed spiral pattern in the center of NGC 615 that ends at a radius of about 30″, farther from the center than two bright knots located at $R = 13''$ and 21″; it is particularly well seen in the I-band residual brightness image. This fact can be treated as an argument in favor of the disk nature of the inner exponential component in NGC 615: to develop stellar spiral arms, the system must be dynamically cold and so must represent a flat thin disk. Curiously, similar spiral arms are seen in the narrowband Hα image of the galaxy that was obtained with the Fabry-Pérot scanning interferometer (Fig. 5). The color map (Fig. 6) evidences that these spirals

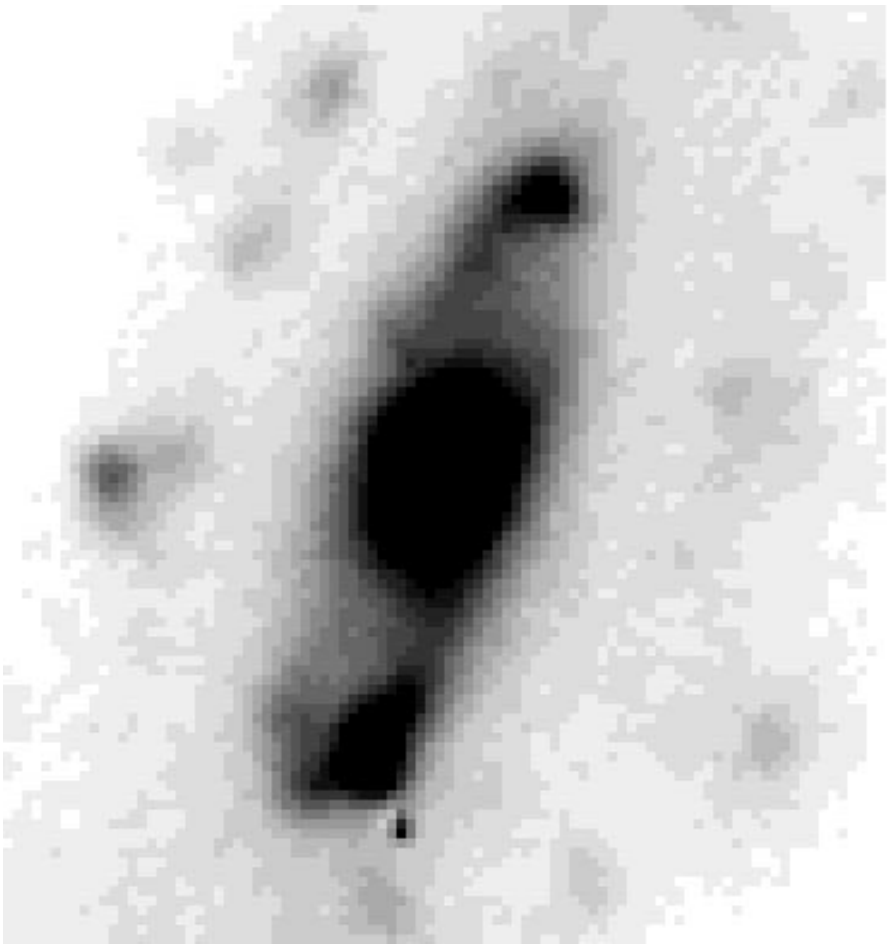


FIG. 5.—Central part of NGC 615 exposed through the narrow (10 Å) filter centered on Hα. The image is direct, P.A. (top) = −36°; the total size of the picture is 61″ × 66″.

are blue in $B-V$ and so may be sites of recent star formation as usual spiral arms seen in outer disks of spiral galaxies.

4. GAS AND STAR KINEMATICS IN THE CENTER OF NGC 615

The observations made with the MPFS of the 6 m telescope have allowed us to construct two-dimensional line-of-sight velocity fields both for stars and ionized gas within the central region 10″ × 15″ of NGC 615. These findings are presented in Figure 7. Similar to the majority of early-type spiral galaxies, NGC 615 lacks a noticeable Hα emission line in its center; it has a LINER-like nucleus, and the most prominent emission line in the optical spectral range inside $R \approx 10''$ is [N II] λ6583. The surface distribution of this emission-line intensity is shown in Figure 7*a*; it is extended and has a quasi-axisymmetric distribution, and its isophotes closely resemble a continuum surface distribution, being only slightly elongated in the line-of-nodes direction. As the emission and continuum morphologies are similar, one would expect the same similarity for the star and gas velocity fields too. Figure 7*b* presents the ionized gas velocity field, and Figure 7*c* the stellar velocity field. Indeed, they do not look too different. Perhaps the gas rotates a little faster. But the shapes of the isovelocities are very similar. Though we would like to have a more extended area covered by velocity measurements, the S-shaped disturbance of the isovelocities seems to be evident.

Since we have two-dimensional velocity distributions, we can check for a circular character of rotation. In the case of planar circular rotation of the ionized gas (or cylindrical rotation of stars), azimuthal variations of a central line-of-sight velocity gradient must obey a cosine law

$$dv_r/dr = \omega \sin i \cos (\text{P.A.} - \text{P.A.}_0) ,$$

where ω is a deprojected central angular rotation velocity, i is the inclination of the rotation plane, and P.A._0 is the orientation of the line of nodes of the rotation plane, coincident, in the case of an axisymmetric ellipsoid (or a thin disk), with the photometric major axis. Given the presence of a bar causing elliptical streaming motions, both major axes, kinematic and photometric, deviate from the line of nodes, and interestingly, they turn in opposite directions (Monnet, Bacon, & Emsellem 1992). So, a comparison of photometric and kinematic major axis orientations allows us to diagnose the axisymmetric—or nonaxisymmetric—character of the rotation.

We have measured azimuthal dependencies of the central line-of-sight velocity gradients for both velocity fields of Figures 7*b* and 7*c* at two different distances from the center, neither in excess of 4″, and we have fitted them by cosine functions by using a least-square method. The phases of the best-fitted cosinusoids that are indeed orientations of the

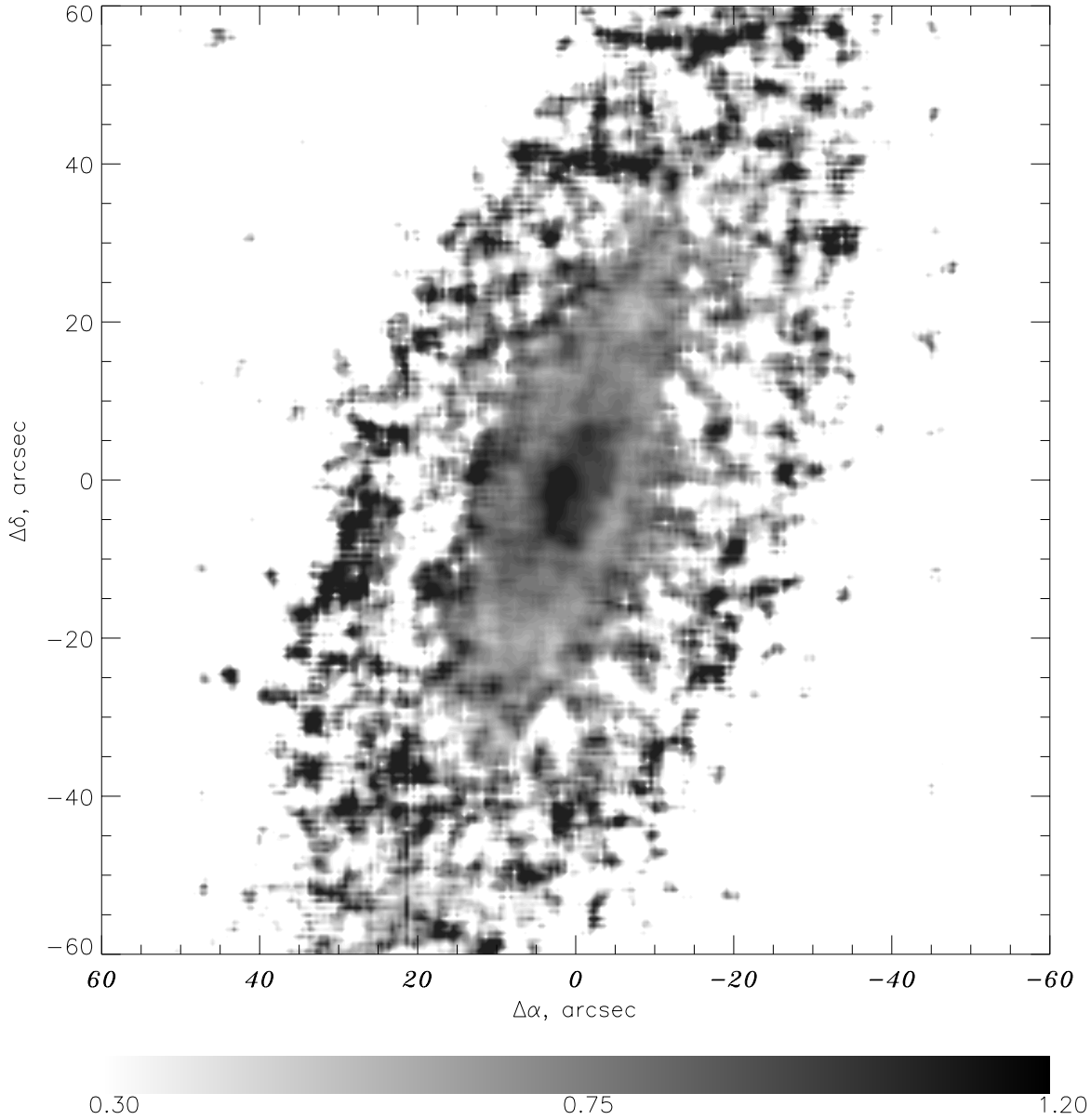


FIG. 6.—$B-V$ color map of NGC 615 according to 2000 October 6 data. The darker regions are redder. The image is direct; north is up, east is left.

kinematic major axes are plotted in Figure 8. One can see that at $R \geq 2''.7$ the position angle of the maximum velocity gradient direction is $\sim 160°$; by referring to Figure 1*b*, we conclude, because the orientation of the photometric major axis is the same, that the rotation of the ionized gas and stars at $R = 2''.7$–$4''$ in NGC 615 is proved to be axisymmetric. At smaller radii, $R < 2''.5$, the kinematic major axis turns by some 11°–17°, and this turn is nearly the same both for the stars and the ionized gas. The photometric major axis (see also Fig. 1*b*) traced under the same seeing quality turns in the same sense as the kinematic major axis; it proves the axisymmetric character of rotation both for stars and ionized gas and implies a presence of inclined circumnuclear disk in the center of NGC 615.

Figure 9 presents long-slit velocity profiles along the major axis for the stars and the ionized gas; within $R = 8''$ we measure the velocities with a step of $0''.8$ along the slit—and farther from the nucleus, with a step of $4''$. A global shape of the rotation curve of NGC 615 is rather common: it is flat at $R \geq 20''$ (2.2 kpc) at the level of some 200 km s^{-1} that is consistent with a width of the 21 cm line integrated over the whole galaxy (Bottinelli et al. 1984). The circumnuclear velocity gradient is higher than average in the radius range $-20''$ to $+20''$: the nucleus is indeed kinematically decoupled, as we reported earlier (Afanasiev et al. 1989). The radius of the decoupled region is $2''$ according to the measurements of the stellar kinematics, which is consistent with our previous results but is somewhat larger, $3''.5$, from the measurements of the gaseous kinematics. Obviously, the size of the kinematically decoupled region is comparable to our spatial resolution element, and this fact causes some uncertainty in our estimates of its radius. We show the central part of the gaseous velocity profile with more details in Figure 10: Figure 10*a* presents a direct view of [N II] emission-line profiles near the center (one can see that they are multicomponent), and Figure 10*b* presents the results of a Gaussian analysis of the [N II] emission line profiles (while in Fig. 9*b* the measurements of the line barycenters are plotted). The Gaussian analysis is more appropriate for the central part of the ionized gas velocity field because the

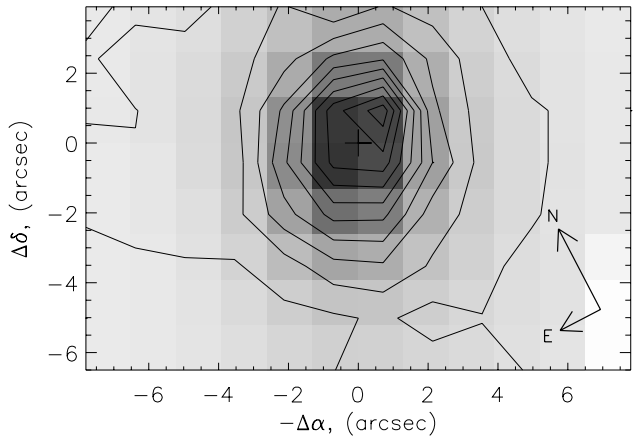


FIG. 7*a*

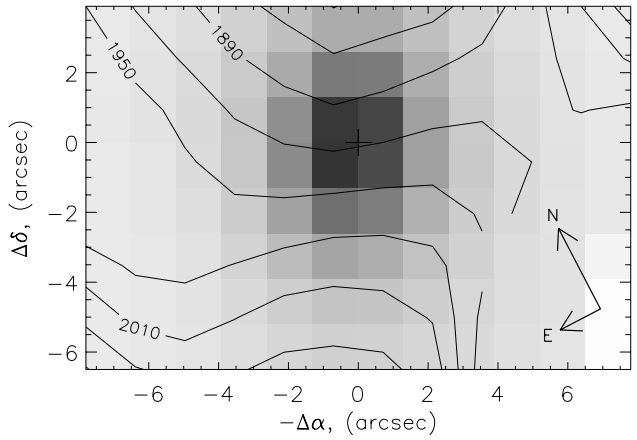


FIG. 7*b*

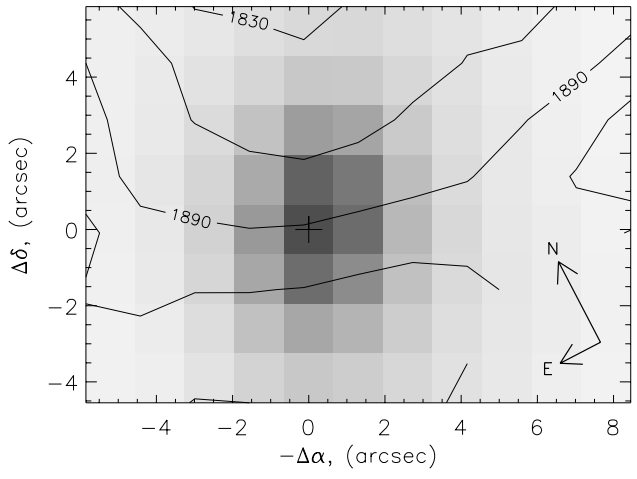


FIG. 7*c*

FIG. 7.—Maps obtained with MPFS for the central part of NGC 615. (*a*) The surface brightness distribution of the emission line [N II] (*contours*) overlaid on the red continuum brightness distribution (*gray scale*); (*b*) isovelocity contours of the ionized gas overlaid on the red continuum brightness distribution; (*c*) isovelocity contours of the stellar component overlaid on the green continuum brightness distribution. The cross marks the photometric (isophotal) center of the galaxy.

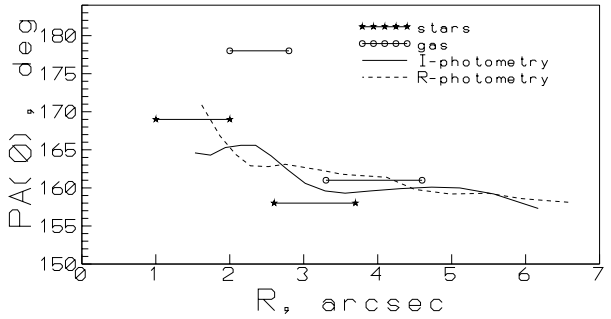


FIG. 8.—Radial variations of the position angles for the dynamical major axis of stars and gas (*signs*) and for the photometric major axis in the *RI* bands (*lines*) according to 2000 October 6 data.

emission lines are double peaked, or at least strongly asymmetric. In general, double-peaked emission-line profiles are usually related to a bar presence in a highly inclined disk (Kuijken & Merrifield 1995). But in such a case the secondary line component traces slower prograde rotation with respect to the primary component behavior. In the case of NGC 615 (Fig. 10*b*) the secondary component "counterrotates" with respect to the primary one, with the similar absolute value of the rotation speed. It is a quite surprising situation because an ionized gas is a dissipational dynamical system. The only reasonable explanation may be that the "counterrotating" gas populates a plane inclined with respect to the plane of the corotating gas. Since the counterrotating gas component is confined to the radii where the bulge dominates and the bulge looks quasi-spheric, perhaps the existence of two gaseous plane rings inside it may be not a crime from the dynamical point of view. However, the origin of such a configuration remains a puzzle.

The combined possibilities of the integral field spectroscopy with MPFS and the long-slit spectroscopy with a rather high spectral resolution have allowed us to obtain a reliable measure of stellar velocity dispersion in the center of NGC 615. Since our derived LOSVDs are very close to pure Gaussians, we have used second moments of Gaussian fitting as a stellar velocity dispersion measure. The instrumental profile width has been determined from the star autocorrelation profile for the MPFS data and from the cross-correlation peak relating to diffuse moonlight for the ESO long-slit data. Figure 11*a* presents a two-dimensional stellar velocity dispersion field obtained with the MPFS, and Figure 11*b* shows the major-axis profiles, both the one simulated from the two-dimensional map and the result of direct long-slit measurements. The two data sets agree quite well. One can see that in the very center $\sigma_* \approx 140$ km s^{-1}, and while the radius increases, it falls rapidly to $\sigma_* \leq 100$ km s^{-1} at $R > 5''$. It is an additional argument in favor of the disk nature of the inner exponential component: this stellar component is dynamically rather cold.

5. STELLAR POPULATIONS IN THE CENTER OF NGC 615

We have measured azimuthally averaged Lick indices Hβ, Mg *b*, Fe5270, and Fe5335 in the radius range 0″–5″ by using the MPFS data, and we have measured the same indices along the major axis in the radius range 0″–17″ by using the ESO long-slit data; the long-slit data at $R > 6''$ are averaged over the 4″ spatial bins. A comparison of two sets of measurements is presented in Figure 12. The agree-

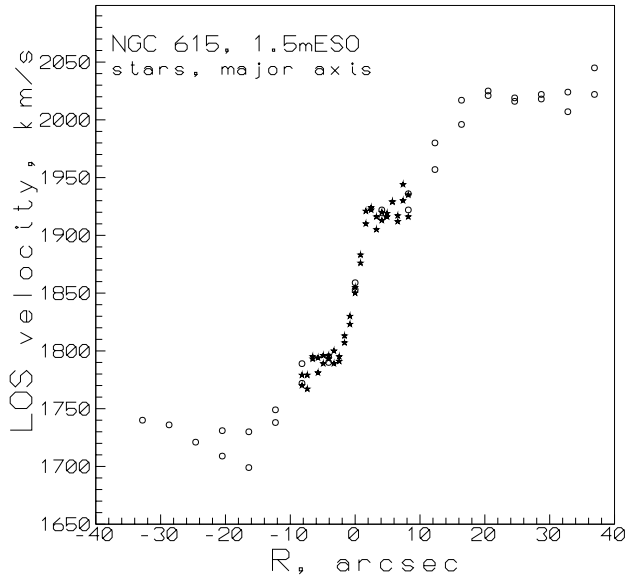


FIG. 9*a*

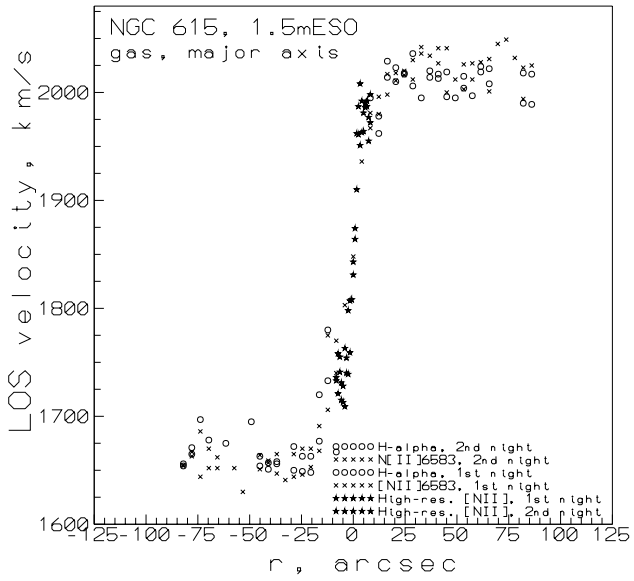


FIG. 9*b*

FIG. 9.—Long-slit major-axis profiles of the line-of-sight velocities for (*a*) stars and (*b*) ionized gas according to our ESO observations. The measurements are made in two radial bins: for $-8'' < R < +8''$, the step along the slit is 0.″82, for outer parts 4.″1. The more prominent signs relate to the 4 hr exposure, the less prominent to the 3 hr one.

ment inside $R = 4''$ is good, especially for Hβ and Mg *b*, despite the different quality of seeing. As we have already found in our earlier investigation of the stellar population properties in the center of NGC 615 (Sil'chenko et al. 1992), there is a drop of metal-line equivalent widths between the unresolved nucleus ($R < 2.''5$) and the bulge. Farther from the center, at $R > 6''$, the metal-line indices return to the nuclear levels and demonstrate a rather flat radial behavior. By reference to the brightness profile subdivisions from Figure 3, we can guess that the shallow index profile seg-

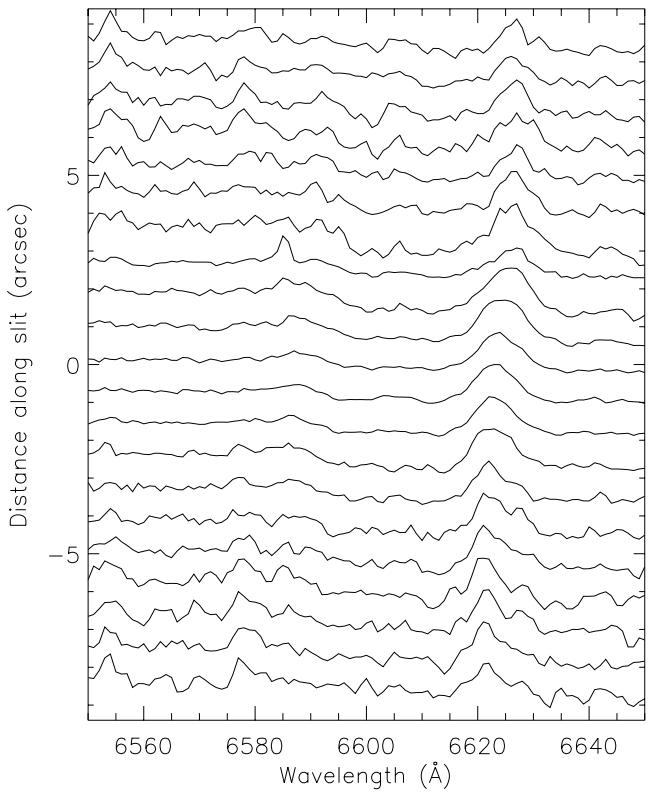


FIG. 10*a*

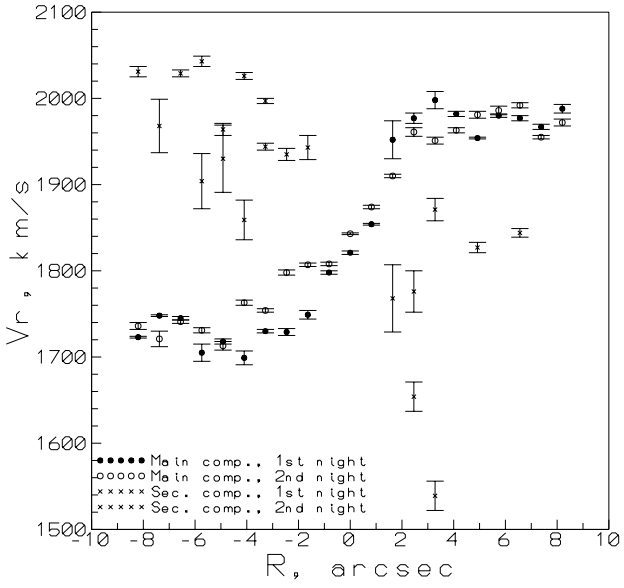


FIG. 10*b*

FIG. 10.—Central part of the long-slit major-axis velocity profile for the ionized gas. (*a*) Direct view of the [N II] λ6583 emission-line profile varying along the slit, with the nucleus in the center; (*b*) the results of Gaussian decomposition of two-component line profiles.

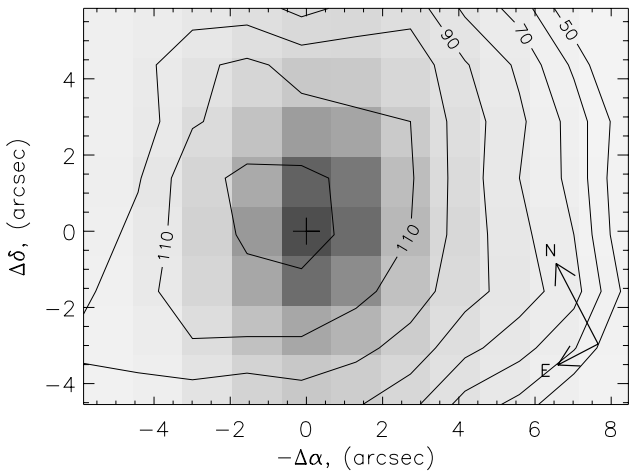


FIG. 11*a*

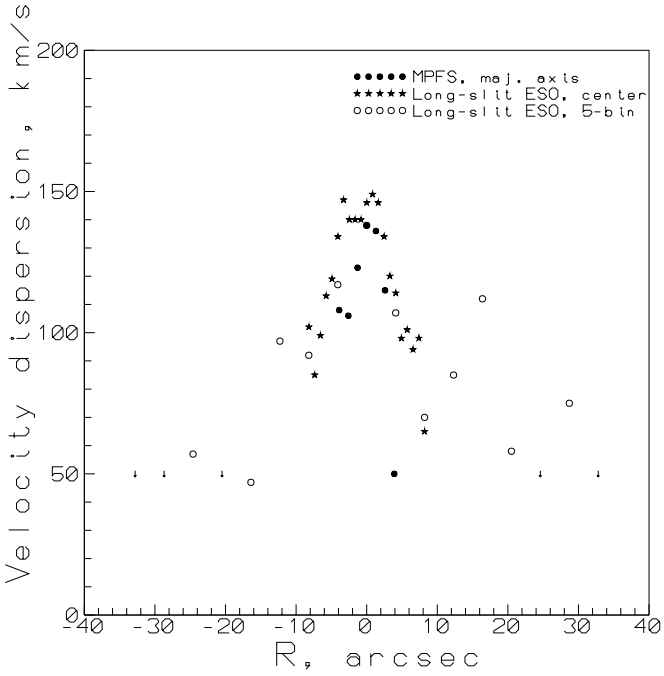


FIG. 11*b*

FIG. 11.—Measurements of the stellar velocity dispersion in the center of NGC 615. (*a*) The two-dimensional map from our MPFS observations, the isolines of the stellar velocity dispersion are superposed on the gray-scale red continuum map; (*b*) the profile of the stellar velocity dispersion along the major axis, simulated MPFS measurements in comparison with the direct long-slit observations.

ments at $R = 7''$–$17''$ correspond to the inner stellar exponential disk of NGC 615, and the intermediate region at $R = 3''$–$5''$ distinguished by low values of all the indices under consideration is a spheroidal component with a quite uncertain brightness distribution that we would refer to as to a "bulge." The characteristics of the nuclear and inner disk stellar populations seem to be similar; the characteristics of the bulge stellar population are different. What are these characteristics, and what is the main difference between the nucleus plus inner disk and the bulge?

In Table 5, we give the Lick indices measured for the nucleus of NGC 615: based on two independent observations, we have been able to estimate their probable errors, which are small. The Balmer emission is practically absent in the very center of the galaxy: we set an upper limit EW(Hα em) ≤ 0.2 Å within $R \approx 5''$, it means that the possible correction of the Lick index Hβ for the emission contamination is less than 0.06 Å. Hence, we can use the Lick index Hβ to determine a mean (luminosity-weighted) age of

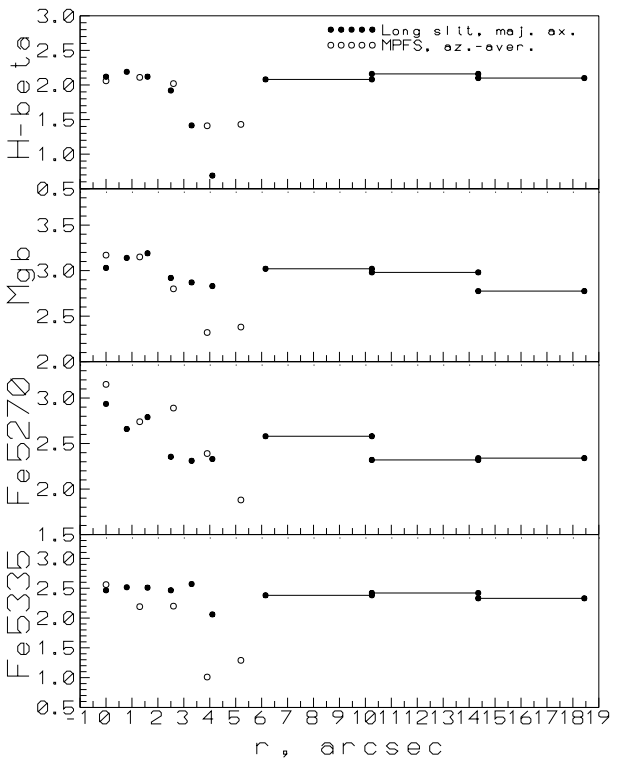


FIG. 12.—Radial profiles of the absorption-line indices Hβ, Mg *b*, Fe5270, and Fe5335; filled circles represent our long-slit measurements along the major axis (at $R > 6''$ binned over $4''$ intervals), and open circles represent our azimuthally averaged MPFS data.

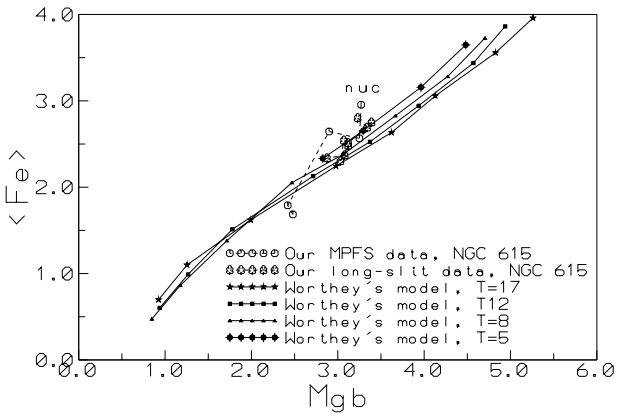


FIG. 13.—The (⟨Fe⟩, Mg *b*) diagram for NGC 615. The MPFS measurements are azimuthally averaged and taken along the radius with the step of 1.″3. The long-slit measurements along the major axis with the steps as in Fig. 12. The ages of the Worthey (1994) models are given in gigayears.

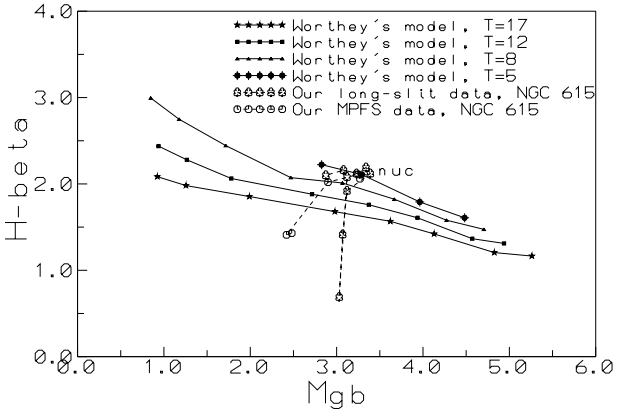


FIG. 14*a*

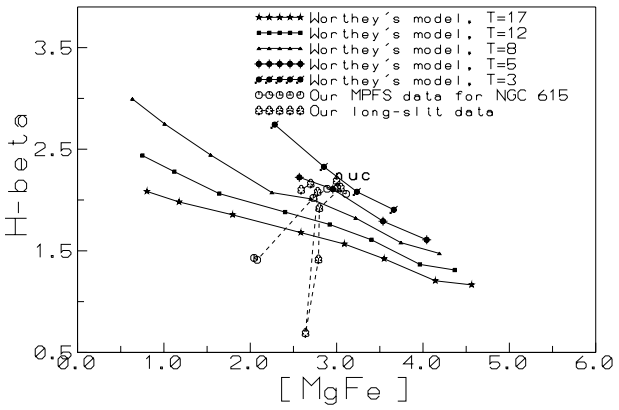


FIG. 14*b*

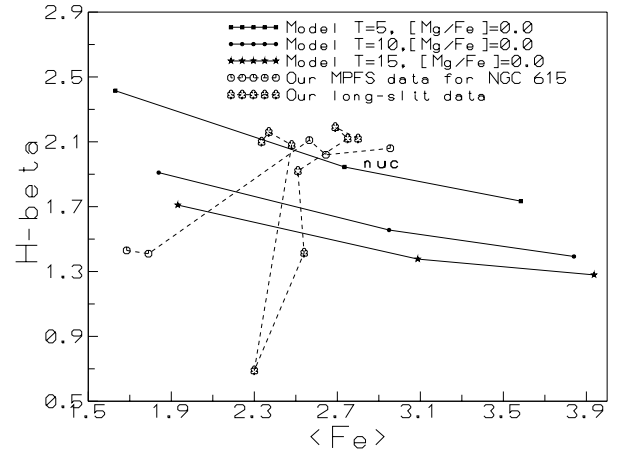


FIG. 14*c*

FIG. 14.—Age-diagnostics diagrams for NGC 615. (*a*) Hβ vs. Mg *b*, models of Worthey (1994); (*b*) Hβ vs. [MgFe], models of Worthey (1994); (*c*) Hβ vs. $\langle$Fe$\rangle$ for [Mg/Fe] = 0, models of Tantalo et al. (1998). The MPFS measurements are azimuthally averaged and taken along the radius with the step of 1.″3, the long-slit measurements along the major axis with the steps as in Fig. 12. The ages of the models are given in gigayears; the metallicities for the Worthey models are +0.50, +0.25, 0.00, −0.22, −0.50, −1.00, −1.50, −2.00, if one takes the signs from right to the left, and for the models of Tantalo et al. they are +0.4, 0.0, and −0.7

the stellar populations. But before do it, we must check if the magnesium-to-iron ratio is solar in NGC 615 because the majority of models are calculated just for this Mg/Fe value. Figure 13 presents the diagram ($\langle$Fe$\rangle$, Mg *b*) in which

TABLE 5

LICK INDICES IN THE NUCLEUS AND OTHER COMPONENTS OF NGC 615

Index	Nucleus, $R = 0''$	Inner Disk, $R = 8''$–$17''$	Bulge, $R = 3.''5$–$5''$
Hβ	2.09 ± 0.03	2.13 ± 0.05	1.42 ± 0.01
Mg *b*.....	3.25 ± 0.02	3.19 ± 0.08	2.45 ± 0.03
$\langle$Fe$\rangle$	2.88 ± 0.08	2.57 ± 0.09	1.74 ± 0.05

the model sequences for the solar Mg/Fe from Worthey (1994) occupy a narrow locus, and any deviation of observational points from this locus can be safely treated as a nonsolar magnesium-to-iron ratio. We know, for example, that elliptical galaxies demonstrate mostly magnesium overabundance being dispersed to the right from the model sequences (Worthey, Faber, & González 1992). The nucleus of NGC 615 represents a quite rare phenomenon: it is located to the left from the model sequences, and so it is marginally iron overabundant. However, this effect is not large: based on the model estimates of Tantalo et al. (1998), who varied the Mg/Fe ratio, we limit the iron overabundance of the nucleus of NGC 615 by roughly 0.1–0.2 dex. The "bulge" and the inner stellar disk are even closer to the model sequence, and if the ages of their stellar populations are about 17 and 5 Gyr, respectively, their magnesium-to-iron ratios may be exactly solar. Taking this consideration into account, we are ready to use (Hβ, metalline index) model diagrams for [Mg/Fe] = 0 to obtain stellar populations ages in NGC 615.

Figure 14 presents three different diagrams for disentangling age and metallicity effects; the model calculations for the solar magnesium-to-iron ratio are taken from Worthey (1994) and from Tantalo et al. (1998). All three diagrams give quite consistent results. The mean age of the nuclear stellar population is obviously slightly less than 5 Gyr. In the radius range of 3″–5″ (two points from the azimuthally averaged MPFS data and one point from the major-axis long-slit data) the mean age of the stellar population increases sharply to more than 15 Gyr, so the spheroidal component called "bulge" is rather old. The inner disk in the radius range of 7″–17″ gives a clump of points between $T = 3$ and 8 Gyr. Since in the inner part of the disk the Balmer emission is insignificant, the age estimate of 5 Gyr for this region is rather precise. Outward the prominence of the Balmer emission increases, up to EW(Hα em) $\approx$ 1 Å at $R \geq 10''$, so the age estimate of 5 Gyr for the outer part of the circumnuclear stellar disk is an upper limit. Recall that at $R \approx 22''$ the intense present star formation is processing now (§ 3). From the age estimates above, we can conclude that though the central spheroidal component is rather old, the nucleus and the inner stellar disk have experienced an intense star formation burst several gigayears ago. Perhaps the late stage of this event continues to be ongoing in the some parts of the inner disk.

6. DISCUSSION

Finally, we can distinguish four structural components in NGC 615, which manifest themselves at different radii. Going from the center outward, they are as follows:

1. $R < 2.''5$–$3''$ (300–350 pc). The inclined (perhaps polar?) circumnuclear fast-rotating disk populated by stars and ionized gas. It can be recognized from a consistent turn

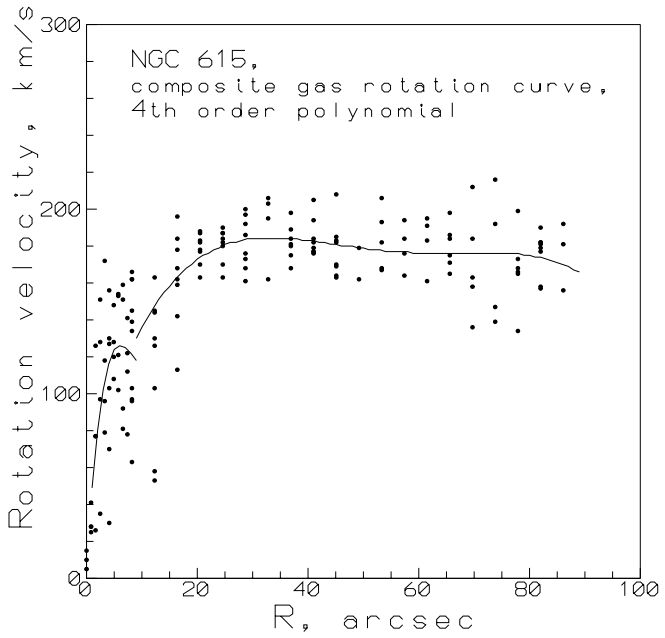


FIG. 15*a*

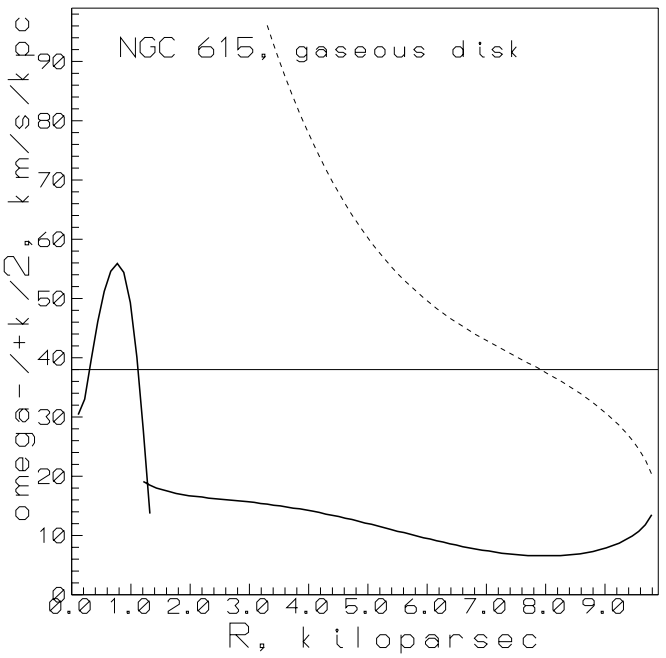


FIG. 15*b*

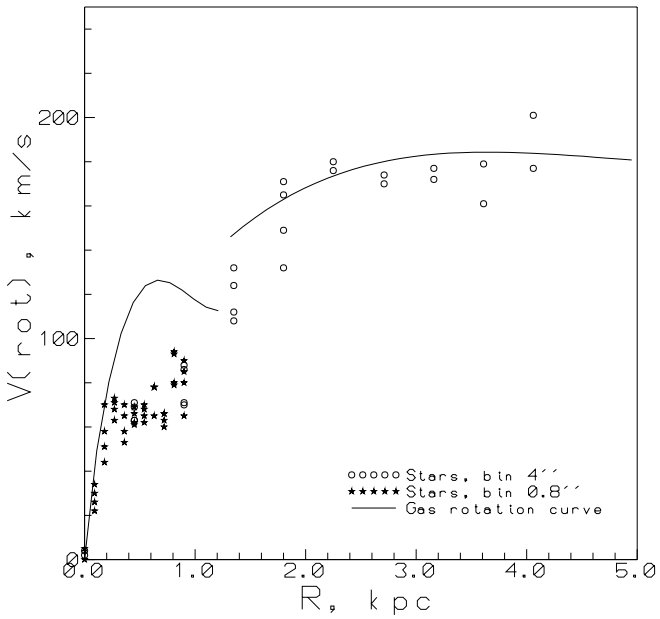


FIG. 15*c*

FIG. 15.—Rotation curves for the stars and ionized gas in NGC 615 from the long-slit data. (*a*) All the measured velocities of the Hα and [N II] emission lines fitted by two segments of fourth-order polynomial; (*b*) possible locations of inner (*solid line*) and outer (*dashed line*) Lindblad resonances according to the rotation curve of the ionized gas; the horizontal line characterizing the pattern speed is selected to match the outer Hα ring at $R = 72''$ (8 kpc) to the outer Lindblad resonance (OLR), then one of the ILRs coincides with the nuclear red ring; (*c*) the measurements for the stellar component are presented by circles and asterisks for both southeast and northwest sides of the major axis; the prominent signs relate to the 4 hr exposure, the less prominent signs to the 3 hr exposure. The gas rotation curve approximated by the fourth-order polynomial as shown in (*a*) is given by a solid line.

of the kinematic and photometric major axes, and it has solar metallicity and a mean stellar population age of about 5 Gyr.

2. $R = 3''$–$6''.5$ (350–750 pc). The compact quasi-spherical bright bulge. It is mildly metal deficient, [Fe/H] ≈ -0.4 to -0.6, and old; dynamically, it demonstrates stellar velocity dispersion above 100 km s^{-1} and stellar rotation twice as slow as that of the ionized gas; the counterrotating gaseous component is present.

3. $R = 8''$–$30''$ (1–3.5 kpc). The inner component, which may be an oval disk. Its photometric major axis is turned with respect to the line of nodes, it is dynamically cold, the stellar rotation matches that of the ionized gas, and the stellar population is mainly 5 Gyr old, but it also contains blue spirals and several bright H II spots within it.

4. $R = 40''$–$70''$ (4.5–8 kpc). The classic outer disk, with an exponential scale length of $\sim$2–3 kpc and central brightness of $B_0 \approx 21.2$ ($I_0 = 18.9$); it is inclined by no more than

60° to the line of sight, and the higher inclinations cited in all catalogs are probably caused by an elliptical ring which borders this disk at $R = 72''$–$75''$ (~ 8 kpc).

As for the rings—one outer at $R > 70''$ (8 kpc) and another marginal at $R \approx 12''$ (1 kpc); see Figure 4—they are usually related to some resonance locations. We do not see a bar in NGC 615, but we perhaps do see some triaxiality if the inner disk is oval. So we would try to set the rings in NGC 615 onto some possible resonances. Figure 15*a* presents a combined gaseous rotation curve derived from our long-slit observations. In the central part, $R \leq 0.2$ kpc, a slope of the rigid-body segment of the rotation curve is consistent with our MPFS data, which indicate $dv_r/dr \approx 300$ km s^{-1} kpc^{-1}. We approximate this rotation curve by two segments of fourth-order polynomials to calculate the $\Omega - \kappa/2$ and $\Omega + \kappa/2$ radial variations, which are plotted in Figure 15*b*. One can see that if we attach the position of the outer ring to the outer Lindblad resonance, we must have two inner Lindblad resonances (ILRs), one of which coincides with the circumnuclear marginal ring. So, our data do not contradict a hypothesis of some triaxiality or a past bar that could produce rings in NGC 615; as Athanassoula (1996) discussed, the rings are more long-living than the bars. The circumnuclear inclined disk in such a picture is located inside the inner ILR and so may be formed from the gas fueled to the center by a triaxial potential. Why it is inclined is a separate question.

Figure 15*c* presents a comparison of gas and stellar rotation. In the radius range of 0.3–1.0 kpc, the stars rotate twice as slowly as the ionized gas. In early-type galaxies, such a discrepancy is often observed in central (bulge-dominated) regions (Fillmore, Boroson, & Dressler 1986), and it is natural when a stellar velocity dispersion is much higher than velocity dispersion of gaseous clouds. Outside $R \approx 1.5$ kpc, the rotation velocities of stars and ionized gas are almost equal; we think that this fact argues against the strong triaxiality of the inner stellar component of NGC 615. Elmegreen et al. (1996) described the following visual properties of ordinary bars in Sb galaxies: their brightness profile along the bar major axis is flat as a result of bright knots at the ends of bar, but being azimuthally averaged, the radial brightness profile is well fitted by a single-scale exponent with very weak, if any, signatures of an extra component in the radius range of the bar. When we calculate the brightness profiles for the inner exponential component, we even mask the "bright knots"; so, even if NGC 615 possesses a bar, it could not cause a change of the profile slope at $R \approx 35''$. So it is not an ordinary bar superposed on a single global disk that is seen in NGC 615; there is a disk within disk, and each was probably formed in a different epoch of global star formation.

The suggestion that NGC 615 possesses an ovally distorted inner disk with a radius of some 3.5 kpc generally does not contradict our early conclusion that circumnuclear ionized gas at radii of $2''$–$3''$ (250–350 pc) may exhibit a circular rotation in the main galactic plane. Shlosman, Frank, & Begelman (1989) described an effect of triaxiality on gas kinematics and distribution and noted that radial gas inflow may result in the formation of a circumnuclear disk with a radius of several hundred parsecs. After subsequent star formation, it may produce precisely the third circumnuclear stellar disk of NGC 615. The continuous accretion of gas from the circumnuclear gaseous disk onto the center may lead to a growth of central mass concentration, which in its turn diminishes the triaxiality. The situation in NGC 615 is very similar to that described by Shlosman et al. (1989).

All the processes related to oval shape formation and destruction and to redistribution of collisional matter in the central region of a galaxy due to the nonaxisymmetry effect have typical durations comparable to a galaxy age, and so they are usually called "secular evolution." NGC 615 belongs to a rather rich group including at least three elliptical and three spiral galaxies as bright as the galaxy itself (Garcia 1993). Close passages and moderate gravitational interactions may be expected in such an environment, and so the bar formation and radial gas redistribution may have been provoked by an external influence. Lin & Pringle (1987) have shown that any gaseous disk that experiences star formation and viscous momentum redistribution with comparable timescales has to establish an exponential density radial profile with the characteristic scale length strictly related to initial sizes of the disk. If we observe two distinct exponential segments of the radial brightness profile in NGC 615 (Fig. 3), those can be related to at least one secondary event when external action may provoke gas redistribution in the disk of the galaxy, or, directly speaking, gas infall into the central region, with a subsequent nuclear star formation burst. Simultaneously, star formation continued in the global gaseous disk but, after the global gas redistribution, with the different, smaller exponential scale length. This is why the properties of the stellar populations in the nucleus and in the inner disk are rather similar.

We thank A. V. Moiseev, postgraduate student of the Special Astrophysical Observatory, for supporting all the observations at the 6 m telescope, and P. A. Chernikov, postgraduate student of the Puschino Radioastronomical Center, for assisting during the observations at the 6 m telescope with the Fabry-Pérot interferometer. A. F. is also grateful to H. Boenhardt from ESO, for his helpful introduction during the observations at the 1.52 m ESO telescope, and to D. Alloin, for the hospitality in the ESO-Santiago computer center. The 6 m telescope is operated with the financial support of the Science Ministry of Russia (registration number 01-43). During the data analysis we used the Lyon-Meudon Extragalactic Database (LEDA), supplied by the LEDA team at the CRAL–Observatoire de Lyon (France), and the NASA/IPAC Extragalactic Database, which is operated by the Jet Propulsion Laboratory, California Institute of Technology, under contract with the National Aeronautics and Space Administration. The work was supported by a grant from the Russian Foundation for Basic Researches 98-02-16196, by the grant of the President of Russian Federation for young Russian doctors of sciences 98-15-96029, and by the Russian State Scientific-Technical Program "Astronomy. Basic Space Researches" (section "Astronomy").

REFERENCES

Afanasiev, V. L., Burenkov, A. N., Zasov, A. V., & Sil'chenko, O. K. 1988, Astrofizika, 28, 243 (English transl. Astrophysics, 28, 142)
Afanasiev, V. L., Vlasyuk, V. V., Dodonov, S. N., & Drabek, S. V. 1996, Multizrachkovyj Spektrograf MPFS: Rukovodstvo Polzovatelya (Nizhnij Arkhyz: Spets. Astrofiz. Obs.)
Afanasiev, V. L., Sil'chenko, O. K., & Zasov, A. V. 1989, A&A, 213, L9
Afanasiev, V. L., Vlasyuk, V. V., Dodonov, S. N., Sil'chenko, O. K. 1990, Multipupil Fiber Spectrograph of the 6-Meter Telescope (SAO preprint 54) (Nizhnij Arkhyz: Spets. Astrofiz. Obs.)
Athanassoula, E. 1996, in ASP Conf. Ser. 91, Barred Galaxies, ed. R. Buta, D. A. Crocker, & B. G. Elmegreen (San Francisco: ASP), 309
Boroson, T. 1981, ApJS, 46, 177
Bottinelli, L., Gouguenheim, L., Paturel, G., & de Vaucouleurs, G. 1984, A&AS, 56, 381
Buta, R. 1993, PASP, 105, 654
Buta, R., & Crocker, D. A. 1993, AJ, 105, 1344
Buta, R., van Driel, W., Braine, J., Combes, F., Wakamatsu, K., Sofue, Y., & Tomita, A. 1995, ApJ, 450, 593
Cardiel, N., Gorgas, J., Cenarro, J., & González, J. J. 1998, A&AS, 127, 597
Courteau, S. 1996, ApJS, 103, 363
de Jong, R. S. 1996, A&A, 313, 45
de Vaucouleurs, G., & de Vaucouleurs, A. 1964, Reference Catalogue of Bright Galaxies (Austin: Univ. Texas Press)
Elmegreen, B. G., Elmegreen, D. M., Chromey, F. R., Hasselbacher, D. A., & Bissell, B. A. 1996, AJ, 111, 2233
Fillmore, J. A., Boroson, T. A., & Dressler, A. 1986, ApJ, 302, 208
Freeman, K. C. 1970, ApJ, 160, 811
Garcia, A. M. 1993, A&AS, 100, 47
Hubble, E. 1926, ApJ, 64, 321
Kormendy, J. 1977, ApJ, 214, 359
———. 1979, ApJ, 227, 714
———. 1984, ApJ, 286, 116
Kuijken, K., & Merrifield, M. R. 1995, ApJ, 443, L13
Landolt, A. U. 1992, AJ, 104, 340
Lin, D. N. C., & Pringle, J. E. 1987, ApJ, 320, L87
Longo, G., & de Vaucouleurs A. 1983, A General Catalogue of Photoelectric Magnitudes and Colors of Galaxies (NSSDC/ADC Cat. 7167) (Austin: Univ. Texas Press)
Mathewson, D. S., & Ford, V. L. 1996, ApJS, 107, 97
Monnet, G., Bacon, R., & Emsellem, E. 1992, A&A, 253, 366
Moriondo, G., Giovanardi, C., & Hunt, L. K. 1998, A&AS, 130, 81
Ryder, S. D., Zasov, A. V., McIntyre, V. J., Walsh, W., & Sil'chenko, O. K. 1998, MNRAS, 293, 411
Shlosman, I., Frank, J., & Begelman, M. C. 1989, Nature, 338, 45
Sil'chenko, O. K. 1994, Doctoral thesis, Moscow State Univ.
Sil'chenko, O. K., & Afanasiev, V. L. 2000, A&A, 364, 479
Sil'chenko, O. K., Afanasiev, V. L., & Vlasyuk, V. V. 1992, AZh, 69, 1121 (English transl. Soviet Astron., 36, 577)
Sil'chenko, O. K., Burenkov, A. N., & Vlasyuk, V. V. 1997, NewA, 3, 15
Sil'chenko, O. K., & Vlasyuk, V. V. 1992, AZh Pisma, 18, 643 (English transl. Soviet Astron. Lett., 18, 255)
Tantalo, R., Chiosi, C., & Bressan, A. 1998, A&A, 333, 419
Véron-Cetty, M. P. 1984, A&AS, 58, 665
Vlasyuk, V. V. 1993, Bull. Spec. Astrophys. Obs., 36, 107
Worthey, G. 1994, ApJS, 95, 107
Worthey, G., Faber, S. M., & González, J. J. 1992, ApJ, 398, 69
Worthey, G., Faber, S. M., González, J. J., & Burstein, D. 1994, ApJS, 94, 687